"Intrinsic" profiles and capillary waves at homopolymer interfaces: a Monte Carlo study

A. Werner, F. Schmid, M. Müller, K. Binder

Institut für Physik, Universität Mainz, D-55099 Mainz, Germany

Abstract. A popular concept which describes the structure of polymer interfaces by "intrinsic profiles" centered around a two dimensional surface, the "local interface position", is tested by extensive Monte Carlo simulations of interfaces between demixed homopolymer phases in symmetric binary (AB) homopolymer blends, using the bond fluctuation model. The simulations are done in an $L \times L \times D$ geometry. The interface is forced to run parallel to the $L \times L$ planes by imposing periodic boundary conditions in these directions and fixed boundary conditions in the D direction, with one side favoring A and the other side favoring B. Intrinsic profiles are calculated as a function of the "coarse graining length" B by splitting the system into columns of size $B \times B \times D$ and averaging in each column over profiles relative to the local interface position. The results are compared to predictions of the self-consistent field theory. It is shown that the coarse graining length can be chosen such that the interfacial width matches that of the self-consistent field profiles, and that for this choice of B the "intrinsic" profiles compare well with the theoretical predictions. Our simulation data suggest that this "optimal" coarse graining length B_0 exhibits a dependence of the form $B_0 = 3.8 \, w_{\text{SCF}}(1 - 3.1/\chi N)$, where w_{SCF} is the interfacial width, N the chain length and χ the Flory-Huggins parameter.

I. INTRODUCTION

Polymer blends [1,2] are examples of systems which can usually be described very well by mean field theories: Due to the chain connectivity, the effective range of interactions between polymers, which is roughly the extension of the chains, becomes very large for high molecular weights, and according to the Ginzburg criterion, the critical region in which critical fluctuations become important is very small as a result [3]. Hence fluctuations can usually be neglected except in the ultimate vicinity of the critical point.

If interfaces are present, however, there exists a type of fluctuations which survives even deep in the two phase region. This is because the interface breaks a continuous symmetry, the translational invariance. As a consequence, long wavelength transversal excitations come into existence (Goldstone bosons). The energy of these "capillary waves" of the local interface position [4] vanishes as the wavelength approaches infinity. These fluctuations are not taken into account in mean field approximations. Nevertheless, they strongly influence all quantities which depend on transversal degrees of freedom.

For example, the interfacial waves contribute to the total width of the interface in a way that it diverges logarithmically with the lateral system size [4]. In other words, the apparent width of the interface depends on the length scale on which the interface is studied. This important observation is not just of academic interest, but also relevant for technical reasons: The mechanical stability of interfaces is to a great extent determined by the number of entanglements between polymers of different type which is, in turn, closely related to the interfacial width on the length scale of at most the radius of gyration R_g. On the other hand, experiments which measure the interfacial width usually work with lateral resolutions characterized by much larger length scales. Hence, the experimental results cannot be directly related to the mechanical properties, and a careful analysis of capillary wave effects is required [5,6].

Despite their success in the description of general bulk thermodynamics, mean field approaches thus apparently fail to capture essential properties of polymer interfaces. However, the situation is not entirely hopeless. Capillary waves are the only Goldstone bosons present in the system, and one may safely assume that they are the only fluctuations which remain important outside of the critical region. Further simplification can be achieved by neglecting the coupling of long wavelength capillary wave fluctuations to the local interfacial structure. This leads to a simple picture in which the interface is described by: [4]

- the local interface position, a function h which parameterizes a two dimensional surface and which is distributed according to a capillary wave Hamiltonian $\mathcal{H}\{h\}$;

- local intrinsic profiles, which are centered around the local interface position, but do not depend on h otherwise, and which can be calculated within an appropriate mean field theory.

The intrinsic profiles characterize the interface on a certain length scale which has yet to be specified, *i.e.*, the coarse graining length. The theory thus assumes that one can define a coarse graining length on which mean field theory provides a valid description of the interfacial structure. If this is the case, it should be related to one of the natural length scales in the system, *i.e.*, the radius of gyration of the chains, the intrinsic width of the interface, or some microscopic length such as the monomer size.

We shall quantify this picture in more detail for the special case of a planar interface. Neglecting bubbles and overhangs, the local interface position can then be parameterized by a single-valued function $h(x, y)$. Long wavelength capillary fluctuations basically cost the free energy associated with the increase of interfacial area. Hence the capillary wave Hamiltonian is given by [5,7,8]

$$\mathcal{H}_{CW}\{h\} = \sigma \int dx\,dy \left\{ \sqrt{1 + \left(\partial h/\partial x\right)^2} \sqrt{1 + \left(\partial h/\partial y\right)^2} - 1 \right\} \approx \frac{\sigma}{2} \int dx\,dy |\nabla h|^2, \tag{1}$$

where σ is the interfacial tension, and $|\nabla h| \ll 1$ has been assumed. Since it is essentially quadratic in h, thermal averages can be carried out easily. The functional $\mathcal{H}_{CW}$ can be diagonalized by means of a Fourier transformation with respect to x and y, resulting in $\mathcal{H}_{CW}\{h\} = \sigma/2 \sum q^2 |h(\vec{q})|^2$, and the thermal average of $h(\vec{q})$ takes the value

$$\langle |h(\vec{q})|^2 \rangle = 1/(\sigma q^2). \tag{2}$$

For the local interface position, one finds a Gaussian height distribution

$$P_L(h) = 1/\sqrt{2\pi s^2} \exp(-h^2/2s^2) \tag{3}$$

with

$$s^2 = \frac{1}{4\pi^2} \int d\vec{q} \langle |h(\vec{q})|^2 \rangle = \frac{1}{2\pi\sigma} \ln(\frac{L}{B_0}).$$

Here $(2\pi/L)$ and $(2\pi/B_0)$ had to be introduced as lower and upper cutoff of the integral $\int d\vec{q} \langle |h(\vec{q})|^2 \rangle \sim \int dq/q$, which diverges both for $q \to 0$ and for $q \to \infty$. The large length L is set by the system size, and the small length B_0 is the coarse graining length mentioned above on which the interface assumes its "intrinsic" structure.

The intrinsic profiles can be calculated using one of the various sophisticated mean field approaches which have been specifically designed to study inhomogeneous polymer systems [9–12]. In our work, we use Helfand's self-consistent field theory, which treats the polymer chains as random walks in the self-consistent field created by the surrounding polymers [9,13]. Given the intrinsic density profile $\rho_{Q,intr}(z)$ of a given quantity Q, the general profile $\rho_Q(x, y, z)$ takes the form $\rho_Q(x, y, z) = \rho_{Q,intr}(z - h(x, y))$, and after performing the thermal average over the capillary wave fluctuations, one obtains the "apparent" profiles (convolution approximation):

$$\rho_{Q,L}(z) = \int dh\, \rho_{Q,intr.}(z - h)\, P_L(h). \tag{4}$$

For example, the interfacial width which we define as

$$w := \rho \left/ \left| \frac{d(\rho_A - \rho_B)}{dz} \right|_{z=h} \right., \tag{5}$$

in a binary (AB) blend, is broadened according to [5,14]

$$w_L^2 = w_{intr}^2 + \frac{1}{4\sigma} \ln(\frac{L}{B}). \tag{6}$$

For polymer interfaces, this relation was originally derived by Semenov [5], who suggested that the coarse graining length is given by $B = \pi w_{intr}$.

The use of a sharp cutoff B in the capillary Hamiltonian is of course not a rigorous procedure. Compared to the length scale B the intrinsic width is not necessarily small, and, hence, it is possible that bulk fluctuations and fluctuations of the local interface position become coupled on this small scale. Furthermore, higher order terms, such as $|\Delta h|^2$, could become important. Thus, a test of the accuracy of the present approach is clearly warranted.

In the present paper, we aim to provide a detailed test of this picture. To this end, we have performed extensive Monte Carlo simulations of interfaces between homopolymer phases in a symmetric binary (AB) homopolymer mixture, using the bond fluctuation model [15–17]. The presence of capillary waves at polymer interfaces has been

2

demonstrated experimentally [7,8] and in Monte Carlo simulations [14,18,19]. In an earlier study, we have established quantitatively the validity of capillary wave concepts for interfaces confined in thin films, and for effectively free interfaces, $i.e.$, in the limit of large film thickness D [14]. Interfacial profiles of various quantities have also been obtained previously from simulations [20] and compared to mean field predictions [21,14,22].

In two of these studies [14,22], capillary waves on length scales down to a given coarse graining length B_0 were subtracted using a coarse graining procedure. However, a direct comparison between self-consistent field calculations and Monte Carlo results or experiments obviously faces the problem that the coarse graining length of the intrinsic profiles is as yet not known. In the previous work [14,22], it was chosen somewhat $ad\ hoc$, such that the measured interfacial width compares well with the calculated width. The way how this "optimal choice" of the coarse graining length depends on the model parameters, $i.e.$, on the various natural length scales in the system, was not investigated.

The present work therefore attempts a systematic study of this coarse graining length, in particular its dependence on the chain length and the chain incompatibility. To this end, we have calculated profiles as a function of the coarse graining length, and performed systematic variations of both the chain length N and the Flory-Huggins parameter χ. As we shall see, our results can be brought into agreement with the self-consistent field profiles when using a coarse graining length which scales roughly like $B \propto w_{\mathrm{SCF}}[1 - 3.1/(\chi N)]$, where w_{SCF} is the width of the self-consistent field profile. This is one of the main results of this work. On the other hand, intrinsic profiles are also interesting in their own right. We shall see for the case of density profiles for contacts within chains and between chains (contact numbers), that the intrinsic profiles may actually differ qualitatively from apparent profiles.

Our paper is organized as follows: In the next section, we introduce the bond fluctuation model and the simulation technique and comment briefly on the self-consistent field calculations. In section III, we analyze the capillary wave spectrum of the interface and demonstrate how it can be used in different ways to extract the interfacial tension σ [22]. Section IV is then devoted to the discussion of various intrinsic profiles and of the coarse graining length. We summarize and conclude in section V.

II. MODEL AND TECHNICAL DETAILS

The bond fluctuation model is a refined lattice model for polymer fluids which has the advantage of combining the computational efficiency of a lattice model with high versatility, such that the actual structure of the fluid shows almost no signature of the structure of the underlying lattice. Polymers are modeled as chains of effective monomers, each occupying a cube (eight sites) of a simple cubic lattice, and these monomers are connected by bonds of variable length of 2, $\sqrt{5}, \sqrt{6}, 3$, or $\sqrt{10}$ lattice constants. At a volume fraction 0.5 or a monomer number density 1/16, the polymer fluid exhibits the characteristic properties of a dense melt, $i.e.$, polymer conformations have almost ideal Gaussian chain statistics [23]. We consider homopolymers made of two different types of monomers – A and B – which interact via a symmetric potential $\epsilon_{AA} = \epsilon_{BB} = -\epsilon_{AB} = -k_BT\epsilon$ if they are less than $\sqrt{6}$ lattice constants apart from each other ($i.e.$, the interaction shell includes 54 neighbor sites). Most simulations were done using polymers of length $N = 32$; the A and B homopolymers then demix at $\epsilon > \epsilon_c \approx 0.014$. However, we increase the chain length up to $N = 256$ in order to investigate the chain length dependence of the coarse graining length B_0. A well-defined interface is enforced in the canonical ensemble in a thick film geometry ($L \times L \times D$), with periodic boundary conditions in the L directions and walls which favor A on one side and B on the other side. The wall interacts with the monomers in the first two layers near the wall, and the interactions were chosen large enough that the walls are wetted by their favorite phase [24] ($e.g.$, for $N = 32$ and $\epsilon = 0.03$, we choose $\epsilon_w = 0.1k_BT$). These boundary conditions ensure that the interface is on average located in the middle of the film. The film thickness ($D = 64$ or 128) is large enough compared to L ($L = 128$) that the capillary wave fluctuations are limited by the system size rather than by the film thickness [14], and that the interactions of the interface with the walls are negligible. Hence the interface is basically free. We equilibrate and sample the system using a combination of local monomer moves [15], slithering snake moves [25], and particle exchange moves. The autocorrelation time in the simulations will be discussed in section III.

In order to analyze the interfacial fluctuations and intrinsic profiles, we split the system into columns of block size $B \times B$ and height D (see Fig. 1) and determine the Gibbs dividing surface $h(x, y)$ in each column [14]. This is done by counting the number of A monomers n_A and of B monomers n_B in the column, and defining $h = N_A\,D/(N_A + N_B)$. Profiles of various quantities are then taken relative to this position. The block size B was varied to allow for a systematic analysis.

The results are compared to self-consistent field predictions within a simple Helfand type theory. In this approach, the polymers are described as random walks with statistical weight

$$\mathcal{P}\{\vec{r}(\cdot)\} = \mathcal{N} \exp\left[-\frac{3}{2b^2}\int_0^N ds \Big|\frac{d\vec{r}}{ds}\Big|^2\right] \qquad (7)$$

in an external field which is created by a monomer interaction potential

$$\beta\mathcal{F} = \frac{1}{\rho_b}\int d\vec{r}\left\{\chi\rho_A(\vec{r})\rho_B(\vec{r}) + \frac{\zeta}{2}(\rho_A + \rho_B - \rho_b)^2\right\} \qquad (8)$$

with the monomer bulk density ρ_b. The basic parameters of the model are the statistical segment length b which characterizes the random walk statistics of the chain, the Flory-Huggins parameter χ which describes the relative repulsion between unlike monomers, and the inverse compressibility $\zeta = 1/(\rho_b k_B T \kappa)$. All these parameters can in principle be determined by independent bulk simulations. The statistical segment length is related to the radius of gyration of the chains, $R_g = b\sqrt{(N-1)/6}$. It depends weakly on the chain length; at fixed $\epsilon N = 0.96$, we find $b(N) = 3.20(5) - 0.8(2)/\sqrt{N}$, and at fixed $\epsilon = 0.03$, $b(N) = 3.11(1) - 0.2(1)/\sqrt{N}$. At chain length $N = 32$ in particular, the statistical segment length takes the value $b = 3.06$. The Flory Huggins parameter depends on the monomer interaction parameter ϵ and on the average number of interchain contacts of a monomer, [27] the "effective coordination number" z_{eff}

$$\chi = 2z_{\text{eff}}\epsilon. \qquad (9)$$

The latter decreases with increasing chain length due to the effect of the correlation hole [12,26]. At fixed $\epsilon N = 0.96$, our data can be described by the law $z_{\text{eff}}(N) = 2.12(1) - 2.97(6)/\sqrt{N}$ which is comparable to the behavior in the athermal system ($\epsilon = 0$): $z_{\text{eff}}(N) = 2.1 - 2.8/\sqrt{N}$ [29]. Finally, the inverse compressibility has been estimated in an athermal system from the entropy density s, $\zeta = 4.1$ [29]. The detailed independent knowledge of the system parameters allows us to compare the simulational results the self-consistent field calculations without adjustable parameter.

III. CAPILLARY WAVES

This section shall be concerned with the analysis of the pure capillary wave spectrum, not bothering yet with intrinsic profiles and coarse graining lengths. A somewhat similar study has already been presented earlier by us [14], hence we shall be brief for the most part. Our analysis is needed here to put our later results into context. In addition, we shall also discuss how the capillary waves can be exploited in different ways to extract the interfacial tension.

The effect of capillary waves on the apparent profiles of the order parameter $m(z) = [\rho_A(z) - \rho_B(z)]/\rho(z)$ is demonstrated in Fig. 2 for different system sizes L. One clearly recognizes how the interface broadens with increasing L. Note that the relaxation time of the capillary waves also grows with the system size and becomes very large, since the forces which drive the capillary waves back are very small for long wavelengths. It is crucial to ensure that the total length of the simulation run is longer than the time scale which governs the dynamics of the slowest capillary mode. In order to check this, we have calculated for each configuration the Fourier modes [18] of the local interface position function $h(x,y)$ in one direction, $h_i = h(\vec{q_i})$ with $\vec{q_i} = (i, 0) \cdot 2\pi/L$. The slowest Fourier mode is the lowest mode with $i = 1$. Thus the quantity of interest is the decay time τ of the corresponding autocorrelation function

$$C_{hh}(t) = \frac{\langle h_1(t) h_1(0)\rangle - \langle h_1\rangle^2}{\langle h_1{}^2\rangle - \langle h_1\rangle^2} \propto \exp(-t/\tau). \qquad (10)$$

It is shown in Fig. 3 for the lateral dimension $L = 128$ as a function of ϵ. The length of the simulation runs was generally between 10^6 and 10^7 Monte Carlo steps. This is much longer than the autocorrelation time τ for small ϵ, but gets close to τ for $\epsilon = 0.1$. Hence, the results for large ϵ have to be interpreted with some caution.

From the capillary wave spectrum, one can now calculate the interfacial tension following three different strategies:

(a) Direct inspection of $h_i{}^2$ as a function of $(1/i)^2$ (Fig. 4a) and use of eqn. (2).

(b) Determination of the width s of the local height distribution function $P_L(h)$ (Fig. 4b) and use of eqn. (3).

(c) Calculation of the apparent interfacial width w_L as a function of system size L (Fig. 4c) and use of eqn (6).

Alternatively to (c), one can also simulate a single (very large) system size L, perform the block analysis described in section II, and study w_B as a function of the block size B. This is shown in Fig. 4d. For very small B, local concentration fluctuations become important and the description by eqn. (6) no longer applies. At large enough B, however, one observes a nice logarithmic dependence, from which only the last point at $B = L$ deviates slightly. The latter can be understood from the fact that the number of capillary modes contributing to the broadening of w_B at $B = L$ is reduced by two compared to that in a larger system ($L > B$), due to the constraint of periodic boundary conditions. [14]

The interfacial tensions obtained with these three different methods are compared with each other and with the theoretical predictions in Fig. 5. The agreement is very good for small values of the Flory-Huggins parameter χ, $\chi < 0.4$ or $\epsilon < 0.07$. At larger incompatibilities, the data scatter very much due to the fact that the order of magnitude of the relaxation time τ (Fig. 3) gets close to the total length of the simulation runs ($5 \cdot 10^6$ Monte Carlo steps). In the same regime, the values of the interfacial tensions derived according to (a), (b), and (c) differ systematically from each other: Those obtained by (b) are lowest, followed by (a) and (c). We cannot excluded that the strategies (a)–(c) yield truly different values for the interfacial tension at high incompatibility χ. Much longer runs would be needed to settle the question whether the deviations are systematic or due to the protracted long correlation times. Systematic deviations are also found close to the critical demixing point, at $\chi < 0.15$ or $\epsilon < 0.03$. Here, critical fluctuations come into play, and the capillary wave description of eqn. (1) does not apply any more on the length scales of the simulation. For comparison, Fig. 5 also shows values of the interfacial tension which have been calculated earlier by some of us using histogram reweighting techniques [20]. Within the statistical error, these independent data agree well with the ones obtained here. The agreement with the theoretical prediction of the self-consistent field calculation is also quite good, especially when the interfacial tension is determined according to (b).

IV. INTRINSIC PROFILES

A. Density profiles and local compressibility

We now turn to the discussion of interfacial profiles. As already emphasized in the introduction, these generally depend strongly on the choice of the coarse graining length or block size B. However, some properties of the interface can also be discussed independently of the coarse graining length: In the approximation (4), capillary waves do not affect the total excess of quantities. This holds in particular for the total density $\rho = \rho_A + \rho_B$: Hence, the total mass reduction in the interfacial area should not depend on the coarse graining length.

To illustrate this, Fig. 6 shows the total density profiles obtained from coarse graining over blocks of different size $B = 8$ or $B = L = 128$. The profiles broaden for larger B, but the depth of the density dip decreases in turn, and the total area remains constant. Also shown is the prediction of the self-consistent field theory for different values of the inverse compressibility ζ. The bulk compressibility of the melt has been determined in earlier work, leading to $\zeta = 4.1$ [29]. However, Fig. 6 indicates that the theoretical profiles calculated with this value are not compatible with the simulation data. Good agreement is reached with $\zeta = 1.9$, *i.e.*, assuming a "local compressibility" at the interface which is more than twice as high than in the bulk. Interestingly, this value of ζ seems to lead to a good description of the simulation data independent of the Flory Huggins parameter χ and the chain length N. This is demonstrated in Fig. 7 for a wide range of monomer interactions ϵ (Fig. 7a) and chain lengths N (Fig. 7b).

In order to further quantify this finding, we plot the depth of the dip in the density profiles at block size $B = 8$ as a function of ϵ in Fig. 8 and compare it with the theoretical prediction for $\zeta = 1.9$ and $\zeta = 4.1$. The block size $B = 8$ was used because the overall shape of the profiles is best fitted by the theory for this choice (cf. section IV.B and Fig. 7). The theoretical prediction for $\zeta = 1.9$ agrees extremely well with the simulation data, even the deviations from the straight line at small ϵ are reproduced quantitatively. In contrast, the prediction for $\zeta = 4.1$ does not fit the data at all.

Hence, it appears that the local density variations at the interface are governed by a local compressibility which differs significantly from the overall compressibility of the melt. The reason for this unexpected finding is not clear. Previous simulation studies of local bulk density fluctuations in a similar system have rather suggested that the compressibility should slightly increase on short length scales [28]. This question will clearly need to be investigated further in future studies.

B. Intrinsic width and "coarse graining length"

Next we consider the density profile $\rho_A(z)$ of a single component which is much more fundamentally affected by the capillary waves. As explained in section II, it is used to locate the interface position and to define the interfacial width w (eqn. (5)). Fig. 4d shows the interfacial width as a function of block size B for various ϵ and fixed chain length $N = 32$, also indicating the predictions of the self-consistent field theory. For all values of ϵ, the theoretical prediction and the simulation results agree best with each other if the block size B is chosen $B = 8$. This is demonstrated even more convincingly in Fig. 9 which compares the interfacial width for block size $B = 8$ and $B = L = 128$ with the self-consistent field results ($\zeta = 1.9$ and $\zeta = 4.1$) over a wide range of Flory-Huggins parameter χ. Except very close to the critical point, the quantitative agreement for $B = 8$ is very good. Note that the theoretical curves for the interfacial width do not depend very strongly on the inverse compressibility ζ. The most notable compressibility effect is observed when plotting w in units of $w_{SSL} = b/\sqrt{6\chi}$. In an incompressible blend, w/w_{SSL} should approach one smoothly from above as χ increases. In a compressible system, it first decreases, reaches a minimum and then rises again. This is found consistently both in the simulations and in the self-consistent field calculations for $\zeta = 1.9$.

We turn to the discussion of the optimal choice of the block size B, which is the coarse graining length for the intrinsic profiles mentioned in the introduction. As discussed there, it should be related to some natural length scale of the system, *i.e.*, some microscopic length like the monomer size or statistical segment length, the intrinsic width, or the radius of gyration of the chains. In the first case, it should be independent of both ϵ and N. In the second case, it should depend on ϵ. So far, we have seen no indication of such a dependence – however, the interfacial width varies so little with ϵ in the range considered by us (Fig. 9) that we cannot draw any conclusions from this observation. In the last case, it should scale like $\sqrt{N}$ with the chain length N.

In order to test the different possibilities, we have performed simulations for chain lengths N of up to 256 , keeping either ϵ constant ($\epsilon = 0.03$) or ϵN constant ($\epsilon N = 0.96$). The resulting interfacial width is shown as a function of block size and compared with the self-consistent field prediction in Fig. 10. One finds that the optimal block size B_0 now differs for the different parameters and depends on the chain length N.

The results are summarized in Fig. 11. At fixed $\epsilon N = 0.96$, *i.e.*, at constant χN, the optimal block size B_0 scales like $B_0 \propto \sqrt{N} \propto 1/\sqrt{\chi}$ (Fig. 11a, inset). This rules out the possibility that B_0 should be related to some microscopic length scale, and establishes a relationship of the form $B_0 = R_g f(\chi N) = w_{\mathrm{SCF}} \tilde{f}(\chi N)$. (Note that $w_{\mathrm{SCF}} \propto R_g/\sqrt{\chi N}\left[1 - \alpha/(\chi N) + \cdots\right]^{-1/2}$ with $\alpha \approx 2.5$ [30,31]). At fixed $\epsilon = 0.03$, *i.e.*, at constant χ, the optimal block size B_0 first increases with N, but levels off faster than $\sqrt{N}$ at the largest chain length $N = 256$ (Fig. 11a). The data seem to approach a constant in the strong segregation limit $N \to \infty$. This long chain length behavior becomes even clearer when plotting B_0/w_{SCF} as a function $1/(\chi N)$ (Fig. 11b). The data can be described satisfactorily by the function

$$B_0 = 3.8 \, w_{\mathrm{SCF}} \left(1 - 3.1 \, (\chi N)^{-1}\right), \tag{11}$$

and all three data sets – those for variable chain length N at fixed incompatibility ϵ (circles), those for variable incompatibility at fixed chain length (stars), and those where the chain length and incompatibility have been varied such that the product ϵN remains constant – collapse onto this single master curve. Hence, our simulational results suggest that the coarse graining length is a multiple of the intrinsic width subjected to strong chain end corrections of order $1/(\chi N)$. Note that the pronounced chain end effects are rather unexpected, because we have used the self-consistent field result in eqn. 11, which already include a correction of a similar form.

Upon increasing the incompatibility at fixed chain length, the interfacial width w_{SCF} decreases, and the chain end correction factor to B_0 increases. Therefore the actual value of the optimal block size B for chain length $N = 32$ has a a maximum at $\chi \approx 0.2$ and varies very little ($B \approx 7$) in the range of χ considered in the previous sections, $\chi \in [0.1 : 0.8]$. This explains why such good results were obtained with constant block size $B = 8$.

Hence, we have shown that our simulation data can be analyzed consistently within the concepts which we have developed in the introduction, *i.e.*, assuming the existence of intrinsic profiles which can be obtained from mean field theory and are broadened by capillary waves.

C. Intrinsic profiles of other quantities

In this last section, we shall discuss selected profiles of other quantities and relate them to self-consistent field predictions. We restrict ourselves to chain length $N = 32$ and calculate the intrinsic profiles by coarse graining over blocks of block size $B = 8$ for a broad range of incompatibilities.

Fig. 12 shows profiles of the relative density of chain ends. They enrich at the interface for entropic reasons. This, in turn, creates a depletion zone at a distance of a radius of gyration from the center of the interface. The height of the peak is slightly underestimated by the theory, yet the overall agreement is still good.

Next we consider the orientational properties of chains. Polymers generally tend to orient themselves parallel to surfaces and interfaces. Two different factors are involved in this behavior: Reorientation of chains without distortion of the intrinsic shape, *i.e.*, at constant absolute value of the radius of gyration or end-to-end vector, and chain compression towards the interface. The self-consistent field theory for Gaussian chains can only handle chain compression, since the x, y and z directions are decoupled in random walks (*i.e.*, the x and y components $R_{ee,x}{}^2$ and $R_{ee,y}{}^2$ are not affected by the presence of the interface.) In our simulations, both effects are present, yet chain compression is by far dominant (Fig. 13 a). The z component of the end-to-end vector is reduced to almost 30 % at the interface. The profiles of $R_{ee,z}{}^2$ are very well reproduced by the self-consistent field calculations, even in details such as the slight overshoot at distances from the interface of about two radii of gyration. The agreement is not quite as good when looking separately at the orientation of chains which are in their minority phase. Close to the interface, $R_{ee,x}{}^2$ and $R_{ee,y}{}^2$ are then found to increase by up to 50 % which indicates that chain reorientation takes place and that the chains are even somewhat stretched parallel to the interface. Deep in the bulk, the total dimensions of minority chains are reduced compared to those of majority chains (Fig. 13b, cf. Sariban and Binder [32]).

Another quantity of interest is the bond orientational parameter q_b which characterizes the orientation of single bonds,

$$q_b = \frac{\langle l_z{}^2 \rangle - (\langle l_x{}^2 \rangle + \langle l_y{}^2 \rangle)/2}{\langle \vec{l^2} \rangle}, \tag{12}$$

where $\vec{l}$ are the bond vectors. The bond orientational parameter is positive for perpendicular orientation and negative for parallel orientation. Fig. 14 shows profiles of q_b for various values of the monomer interaction strength ϵ. Like whole chains, single segments also orient parallel to the interface, but to much less extent [20]. Segment orientations are not accessible to self-consistent field studies of Gaussian chains since random walks do not have well-defined tangent vectors. In order to calculate them, one has to resort to a different chain model, *e.g.*, the wormlike chain model which describes chains as strings of fixed contour length with a conformational weight functional governed by a bending rigidity η [33,34]. The latter is related to the statistical segment length *via* $b = \sqrt{2\eta}\, a$, where a is the monomer length. In the case of the bond fluctuation model, subsequent bonds are essentially uncorrelated except for the fact that they cannot fold back onto themselves. Hence $b \approx a$ or $\eta \approx 1/2$ seems like a reasonable guess for the effective bending stiffness. Bond orientational profiles have been calculated earlier within the wormlike chain model for $\epsilon = 0.1$ and various values of η [21]. At $\eta = 0.5$, the minimum of q_b at the center of the interface takes the value $q_b = -0.025$, *i.e.*, it underestimates the simulations by a factor of two. Better agreement for all ϵ is reached with $\eta = 1.2$. However, such a high bending stiffness would imply that the monomer length is unreasonably small, $a = 1.97$ which is smaller than smallest possible bond length 2 in the bond fluctuation model. The average bond length is $\sqrt{\langle l \rangle^2} = 2.62$. Thus one is lead to suspect that the wormlike chain model does not describe the chains of the bond fluctuation model any better than the Gaussian chain model. Note that the wormlike chain model reduces to the Gaussian chain model in the limit $\eta \to 0$ [34]. However, taking account of the detailed chain architecture in the mean field framework better agreement could be achieved [22].

Finally, we shall examine the profiles of the average contact number density for contacts between monomers of different chains N_{inter} and between monomers of the same chain N_{intra}. One of the fundamental assumptions of the mean field theory is that they should behave like ρ^m where ρ is the total density of monomers, and m is the number of polymer chains involved in a contact, hence $N_{inter} \propto \rho^2$ and $N_{intra} \propto \rho$. Every deviation from this "trivial" dependence thus also indicates a deviation from mean field theory. Note that the ratio N_{inter}/ρ in the bulk phases is the effective coordination number z_{eff} which we have used throughout this paper to calculate the Flory-Huggins parameter χ from the interaction strength ϵ (eqn. (9)). The profiles of $N_{inter}(z)/\rho(z)^2$ and $N_{intra}(z)/\rho(z)$ are shown for various ϵ in Fig. 15. According to the mean field assumption mentioned above, these quantities should be constant. In the simulations, they have a rather complex structure. Generally, the chains rearrange in the vicinity of an interface as to increase the number of intrachain contacts at the expense of the interchain contacts. Right at the center of the interface, however, the trend is opposite: The relative number of interchain contacts has a maximum, and the number of intrachain contacts decreases. This is presumably caused in part by the enrichment of chain ends at the interface. Furthermore, an additional entropic effect comes into play very close to a sharp interface: Two monomers of the same chain which are in contact are connected by a closed loop. If they are located in the immediate vicinity of a sharp interface, the loop can only extend into a half space which is entropically much less favorable than if the full space were available like further away from the interface. Thus, the number of intrachain contacts is reduced at

the interface. We note that this fine structure of contact number profiles has not been observed in previous studies of interfacial structures which did not separate intrinsic profiles from capillary waves [20]. Hence, this is the example of a case where intrinsic profile differ qualitatively from their capillary wave broadened counterpart. Otherwise, the capillary broadening does not affect the qualitative shape of the profiles.

V. CONCLUSIONS

In this paper, we have presented extensive Monte Carlo simulations of homopolymer interfaces, and analyzed them within the framework of a theory [4] which conceives the interface as a two dimensional surface embedded in space and decorated by intrinsic profiles which can be obtained by mean field theory. We have shown that our results are compatible with such a picture. The intrinsic profiles are in good agreement with those obtained from the self-consistent field theory on the length scale of a "coarse graining length" B_0. The comparison between Monte Carlo simulation and self-consistent field calculations indicate that this length scale exhibits a dependence of the form $B_0 = 3.8\, w_{\mathrm{SCF}}(1 - 3.1/\chi N)$. In the long chain length limit this behavior is in qualitative agreement with the suggestion of Semenov [5] $B = \pi w$, however, we find pronounced chain end corrections. We have to note that our raw simulation data do not inevitably lend themselves to such an interpretation. Nothing in the curves shown in Fig. 10 indicates that there should be anything special about the self-consistent field width w_{SCF}, or about the coarse graining length B for which $w_B = w_{\mathrm{SCF}}$. The capillary wave description seems to be valid down to length scales much smaller than that, down to block sizes of about $B \approx 4$. It is conceivable that the interface on these length scales can still be described by intrinsic profiles which would then have nothing to do with the self-consistent field prediction. On the other hand, the local interfacial structure will presumably not decouple from the fluctuations of the interfacial position on length scales smaller than the extension of the chains, and something analogous to the convolution approximation is rather unlikely to be valid. This point will need further consideration in the future. So far, the main merit of our analysis is to have provided insight on the validity range of the self-consistent field theory, and on the length scale on which it is applicable. A theory describing the local interfacial structure on length scales much smaller than w_{SCF} has yet to be tested and established. For example, the P-RISM theory by Schweizer and Curro [12] which puts much more emphasis on the local liquid structure, is possibly a promising candidate. Such a theory will also hopefully contribute to clarify the reason for the rather high negative excess of total density in the interfacial region, which we have discussed in section III.1.

ACKNOWLEDGMENTS

[1] D.R. Paul and S. Newman, *Polymer Blends*, Academic Press, New York (1978); K. Šolc (edt.), *Polymer Compatibility and Incompatibility*, Harwood Academic Publishers, Chur (1980); D.S. Walsh, J.S. Higgins, and A. Maconnachie, *Polymer Blends and Mixtures*, Martinus Nijhoff Publishers, Dordrecht (1985); E.L. Thomas (edt.), *Materials Science and Technology, Vol. 12: Structures and Properties of Polymers*, VCH, Weinheim (1993).

[2] K. Binder, *Adv. Polymer Sci.* **112**, 181 (1994).

[3] V.L. Ginzburg, *Sov. Phys. Solid state* **1**, 1824 (1960); K. Binder, *Phys. Rev.* **A 29**, 341 (1984).

[4] F. P. Buff, R. A. Lovett, F. H. Stillinger, *Phys. Rev. Lett.* **15**, 621 (1965); J. D. Weeks, *J. Chem. Phys.* **67**, 3106 (1977); D. Bedeaux, J. D. Weeks, *J. Chem. Phys.* **82**, 972 (1985).

[5] A.N. Semenov, *Macromolecules* **26**, 6617 (1993); ibid **27**, 2732 (1994).

[6] K.R. Shull, E.J. Kramer, *Macromolecules* **23**, 9769 (1990).

[7] T. Kerle, J. Klein, and K. Binder, *Phys. Rev. Lett.* **77**, 1318 (1996); T. Kerle, J. Klein, and K. Binder, submitted to *Eur. Phys. J.*.

[8]   M. Sferrazza, C. Xiao, R.A.L. Jones, D.G. Bucknall, J. Webster, and J. Penfold, *Phys. Rev. Lett.* **78**, 3693 (1997).

[9]   E. Helfand and Y. Tagami, *J. Polym. Sci., Polym. Lett.* **9**, 741 (1971); *J. Chem. Phys.* **56**, 3592 (1971); ibid **57**, 1812 (1972); E. Helfand. *J. Chem. Phys.* **62**, 999 (1975).

[10] P.J. Flory, *Principles of Polymer Chemistry*, Cornell University Press, Ithaca (1953); *J. Chem. Phys.* **10**, 51 (1942); M.L. Huggins, *J. Phys. Chem.* **46**, 151 (1942).

[11] J. Dudowicz and K. F. Freed, *Macromolecules* **23**, 1519 (1990); H. Tang and K.F. Freed, *J. Chem. Phys.* **94**, 1572 (1991); M. Lifschitz and K.F. Freed, *J. Chem. Phys.* **98**, 8994 (1993); K. F. Freed, *J. Chem. Phys.* **103**, 3230 (1995); K.W. Foremann and K.F. Freed, *J. Chem. Phys.* **106**, 7422 (1997).

[12] K. S. Schweizer and J. G. Curro, in *Advances in Chemical Physics*, Vol XCVIII, I. Prigogine and S. A. Rice (eds.), Wiley, New York(1997).

[13] For a recent review see F. Schmid, *Journal of physics: Condensed matter*, preprint 1998.

[14] A. Werner, F. Schmid, M. Müller, and K. Binder, *J. Chem. Phys.* **107**, 8175 (1997).

[15] I. Carmesin and K. Kremer, *Macromolecules* **21**, 2819 (1988); *J. Phys. (France)* **51**, 915 (1990).

[16] K. Binder (edt.), *Monte Carlo and Molecular Dynamics Simulations in Polymer Science*, Oxford University Press, Oxford (1995).

[17] M. Müller and F. Schmid, in *Annual Reviews of Computational Physics*, D. Stauffer edt., World Scientific, Singapore, preprint 1998.

[18] M. Müller and M. Schick, *J. Chem. Phys.* **105**, 8885 (1996).

[19] M.D. Lacasse, G.S. Grest, and A.J. Levine, *Phys. Rev. Lett.* **80**, 309 (1998).

[20] M. Müller, K. Binder, and W. Oed, *J. Chem. Soc. Faraday Trans.* **91**, 2369 (1995).

[21] F. Schmid and M. Müller, *Macromolecules* **28**, 8639 (1995).

[22] M. Müller and A. Werner, *J. Chem. Phys.* **107**, 10764 (1997).

[23] W. Paul, K. Binder, D.W. Heermann, and K. Kremer, *J. Phys. II (France)* **1**, 37 (1991).

[24] M. Müller and K. Binder, *Macromolecules* 1998, in press.

[25] K. Kremer and K. Binder, *Comp. Phys. Rep.* **7**, 261 (1988).

[26] P.G. de Gennes, *Scaling Concepts in Polymer Physics*, Cornell University, Ithaca (1979).

[27] M. Müller and K. Binder, *Macromolecules* **28**, 1825 (1995).

[28] J. Baschnagel and K. Binder, *Physica* A **204**, 47 (1994).

[29] M. Müller and W. Paul, *J. Chem. Phys.* **100**, 719 (1994).

[30] D. Broseta, G.H. Fredrickson, E. Helfand, and L. Leibler *Macromolecules* **23**, 132 (1990).

[31] H. Tang and K.F. Freed, *J. Chem. Phys.* **94**, 3183 (1991).

[32] A. Sariban and K. Binder, *J. Chem. Phys.* **86**, 5859 (1987); *Macromolecules* **21**, 711 (1988).

[33] O. Kratky and G. Porod, *Rec. Trav. Chim.* **68**, 1106 (1949); N. Saito, K. Takahashi, and Y. Yunoki, *J. Phys. Soc. Jpn.* **22**, 219.(1967).

[34] D.C. Morse and G.H. Fredrickson, *Phys. Rev. Lett.* **73**, 3235 (1994).

L: system size   B: block size
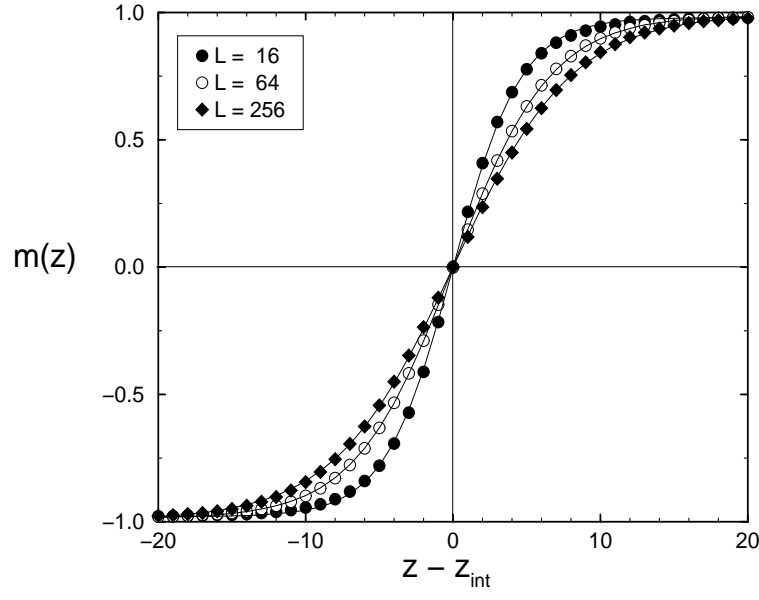
FIG. 1.

Block analysis, schematic picture.
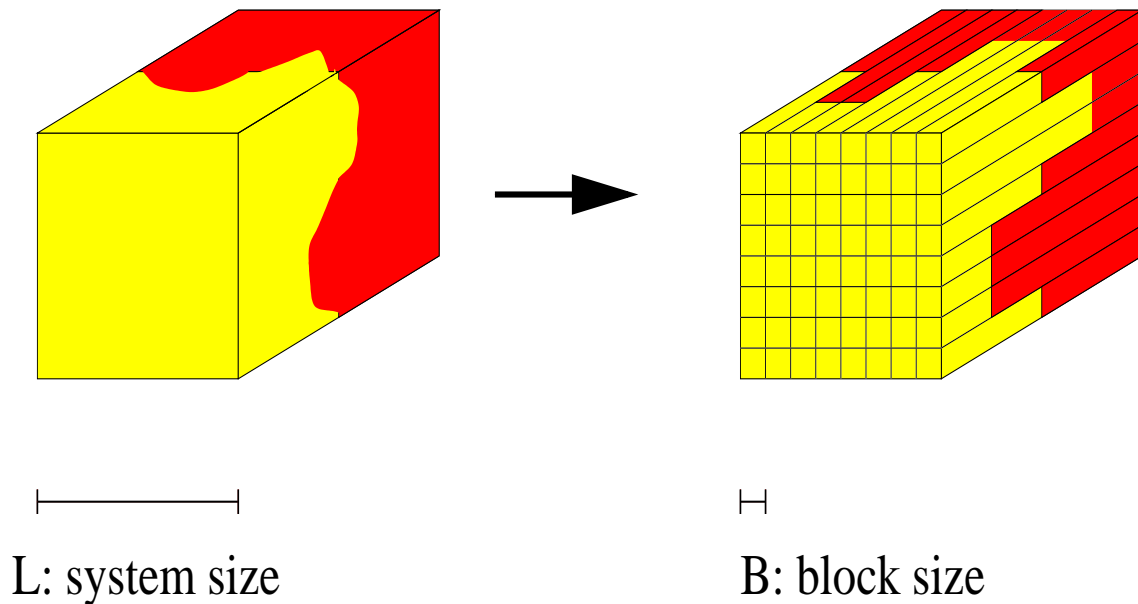
FIG. 2.

Apparent order parameter $m(z) = [\rho_A(z) - \rho_B(z)]/[\rho_A(z) + \rho_B(z)]$ vs. distance from the interface position $z - z_{int}$ in units of the lattice constant, for different system sizes L. Lines are fits to a tanh profile $m(z) = m_b \tanh[(z - z_{int})/w]$. Parameters are $\epsilon = 0.03$ and $N = 32$
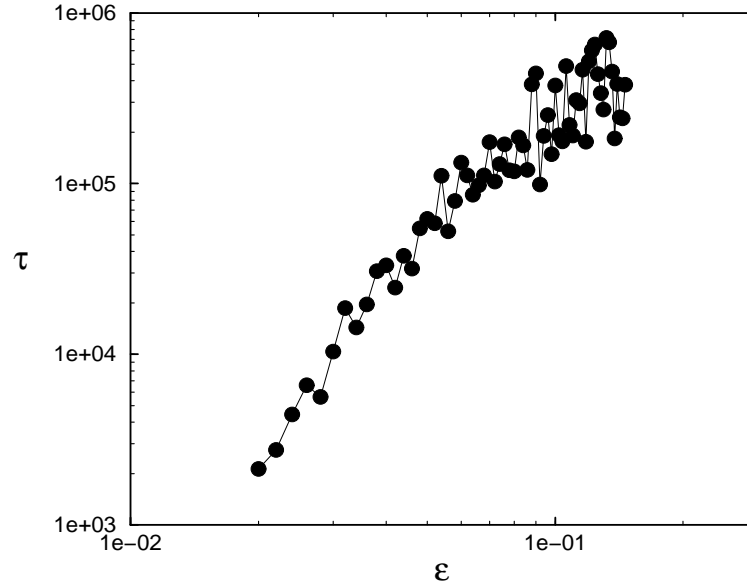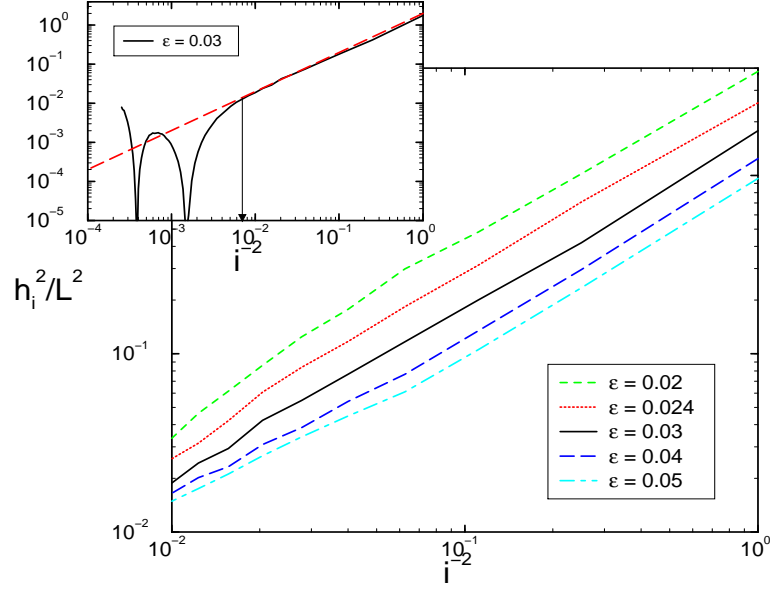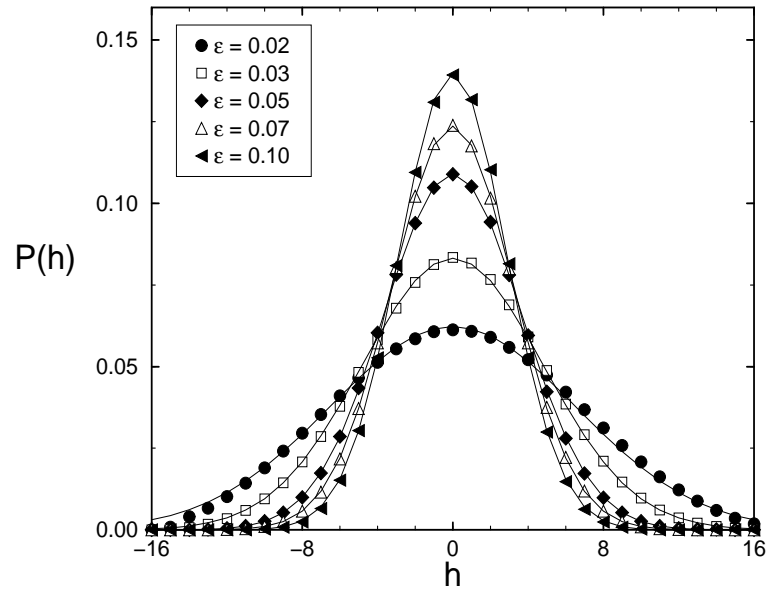

FIG. 3.

Autocorrelation time τ of the slowest capillary wave mode in units of Monte Carlo steps as a function of ϵ for chain length $N = 32$. Four Monte Carlo steps correspond to one local hopping attempt per monomer, three slithering snake trials per chain and 0.1 canonical particle exchange moves.

(a)

(b)

(c)
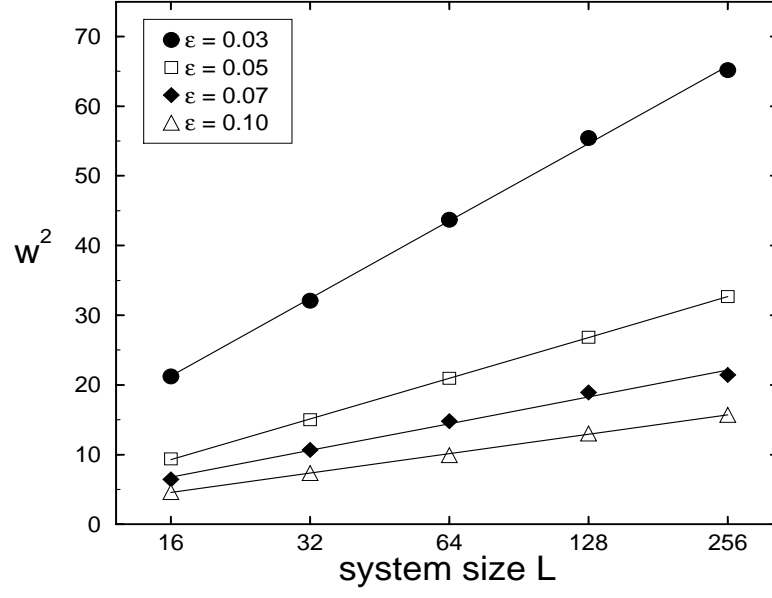
(d)
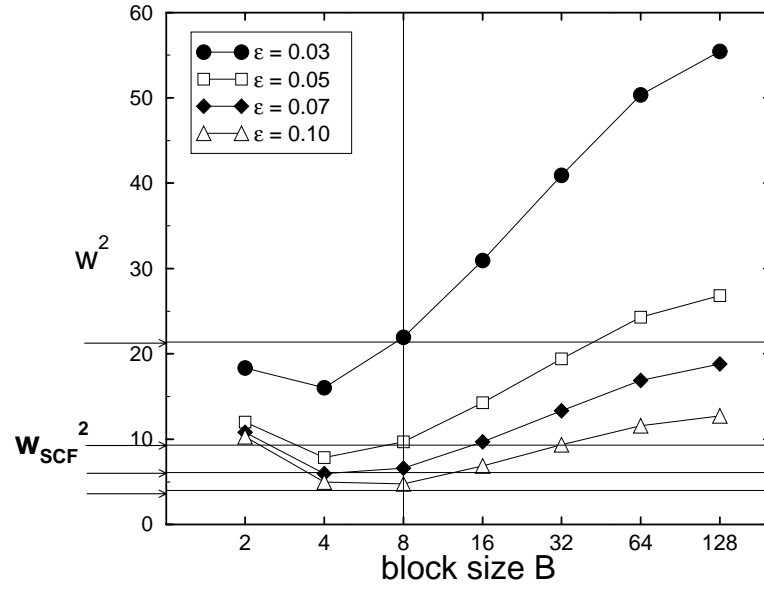
FIG. 4.

FIG. 4

Illustration of different strategies to extract the interfacial tension σ from the capillary wave spectrum. Chain length is $N = 32$, film thickness $D = 64$ (c) and $D = 128$ ((a),(b), and (d)), system size $L = 128$ except in (c), and ϵ varies as indicated. Lengths are given in units of the lattice constant.

(a) Double logarithmic plot of the amplitude h_i^2 of the ith Fourier mode in units of $1/L^2$ vs. $1/i^2$. Inset shows the whole spectrum for $\epsilon = 0.03$. The capillary wave regime sets in at $L/i = 10.7$ (arrow). The theoretical prediction in this regime is $\langle |h_i|^2 \rangle = [L/2\pi i]^2 \sigma^{-1}$ (dashed line, inset).

(b) Distribution $P(h)$ of the local interface position at block size $B = 8$. Lines are fits to a Gaussian distribution $P(h) \propto \exp(-h^2/2s^2)$. The theoretical prediction is $s^2 = 1/(2\pi\sigma) \ln(L/B)$.

(c) Apparent interfacial width w^2 as a function of system size L. Lines are fits to the theoretical prediction $w_L^2 = w_{intr.}^2 + 1/(4\sigma) \ln(L/B)$.

(d) Apparent interfacial width w^2 as a function of block size B. Arrows show the self-consistent field prediction w_{SCF}.
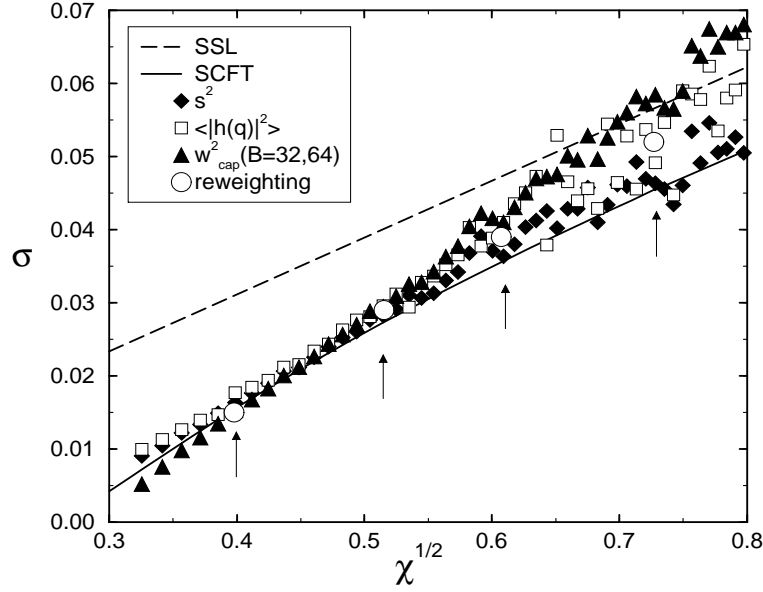
FIG. 5.

Interfacial tension σ in units of $[$ lattice constant $]^{-2}$ as a function of Flory-Huggins parameter χ, as obtained with the different methods illustrated in Fig. 4. Also shown are independent values from Müller *et al* [20], measured from bulk simulations with histogram reweighting techniques. The solid line shows the self-consistent field prediction and the dashed line the strong segregation limit $\sigma_{SSL} = \rho b \sqrt{\chi/6}$.
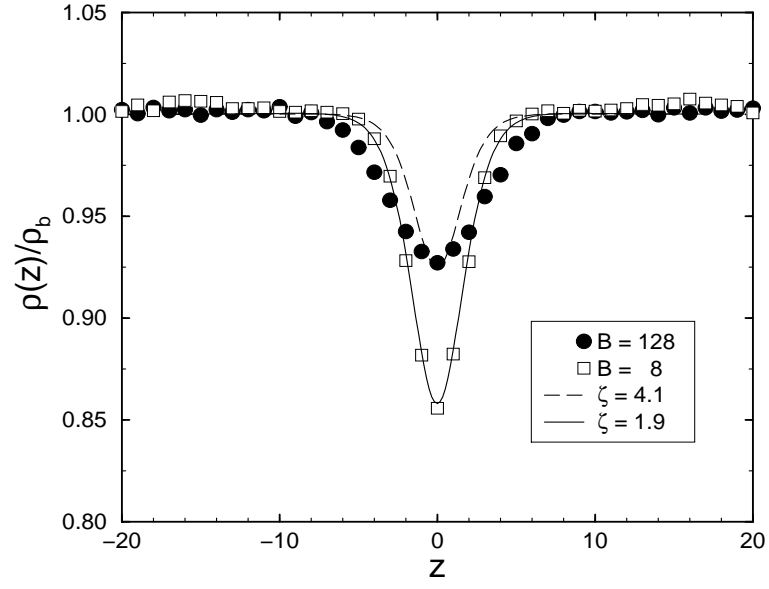
FIG. 6.

Total density profile $\rho(z)$ in units of ρ_b vs. z in units of the lattice constant as measured at block size $B = 8$ (open squares) and $B = L = 128$ (filled circles). Lines show the self-consistent field prediction for the compressibility parameter $\zeta = 4.1$ (dashed) and $\zeta = 1.9$ (solid). Parameters are $N = 32$ and $\epsilon = 0.1$.
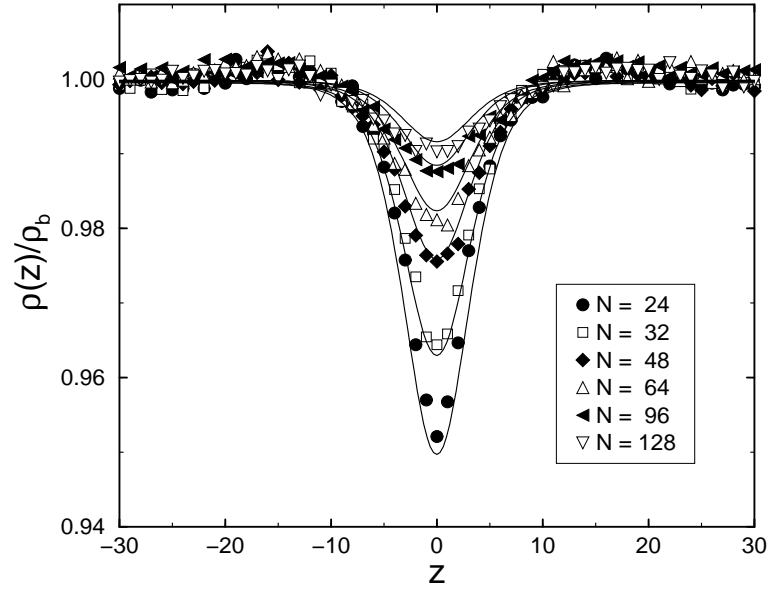
14

(a)
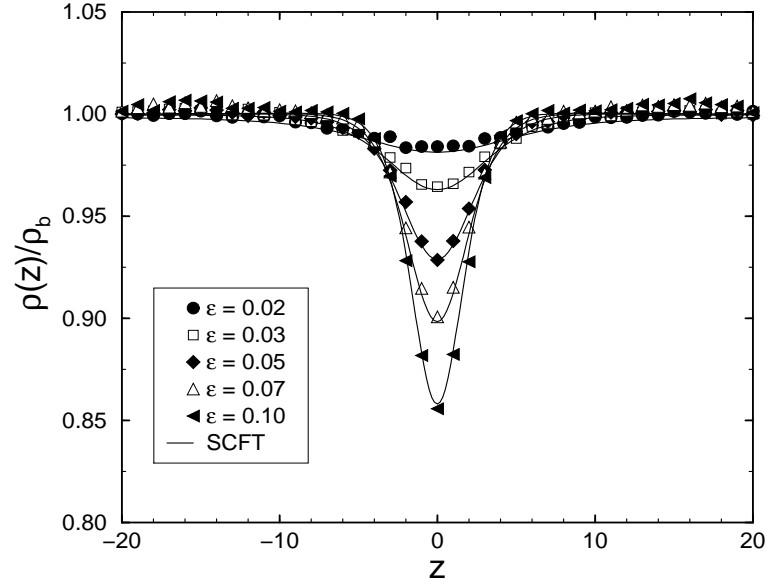
(b)

FIG. 7.

Total density profiles for block size $B = 8$ (a) at chain length $N = 32$ for different ϵ (b) at fixed $\epsilon N = 0.96$ for different N. Lines show the predictions of the self-consistent field theory using $\zeta = 1.9$.
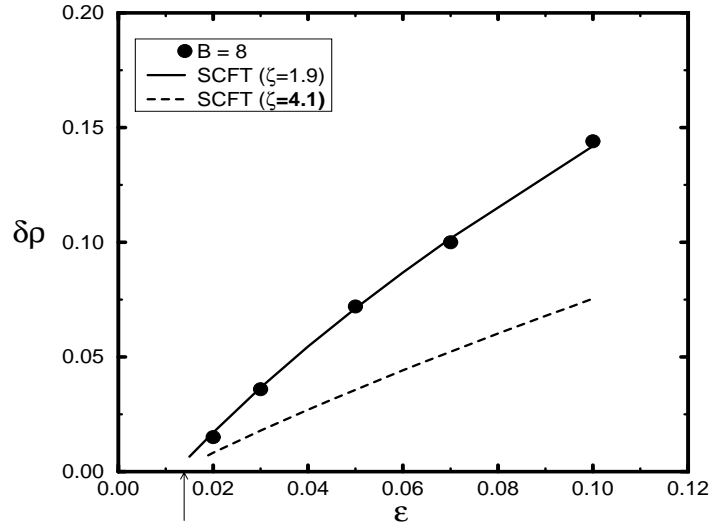
FIG. 8.

Depth of the density dip $\delta\rho = 1 - \rho(0)/\rho_b$ vs. ϵ for the profiles obtained at block size $B = 8$ (Fig. 7a), compared to the self-consistent field prediction for $\zeta = 1.9$ (solid line) and $\zeta = 4.1$ (short dashed line). The arrow indicates the critical demixing value of ϵ.

(a)
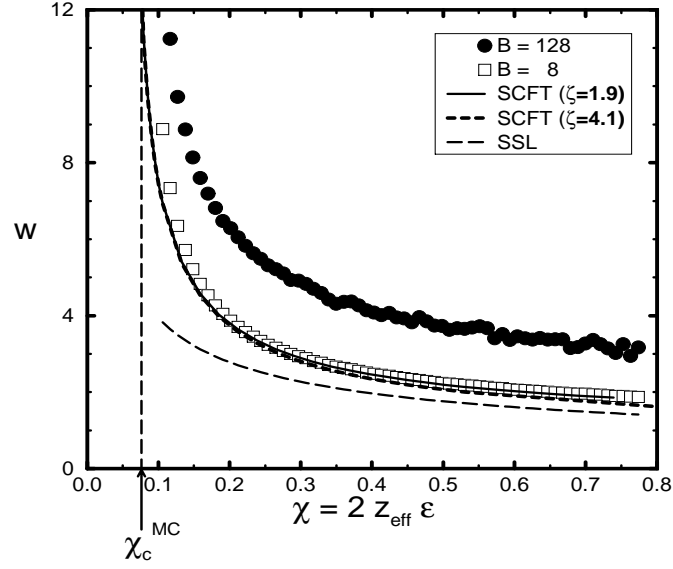
(b)
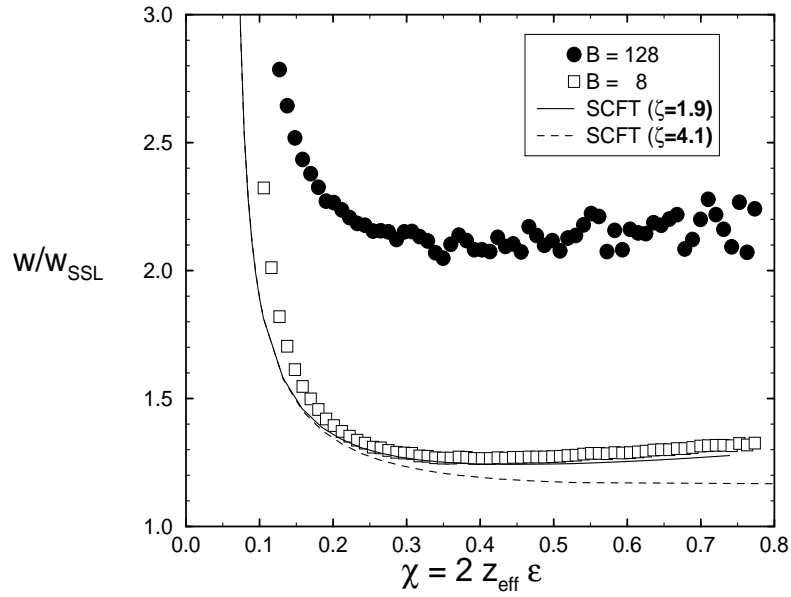
FIG. 9.

Interfacial width w in absolute units (lattice constant) (a) and in units of $w_{SSL} = b/\sqrt{6\chi}$ (b) at block size $B = 8$ (open squares) and $B = L = 128$ (filled circles) vs. Flory-Huggins parameter χ. Lines show the theoretical prediction of the self-consistent field theory at $\zeta = 1.9$ (solid), $\zeta = 4.1$ (short dashed), and the strong segregation limit w_{SSL} (long dashed). Arrow indicates critical demixing value χ_c.

(a)
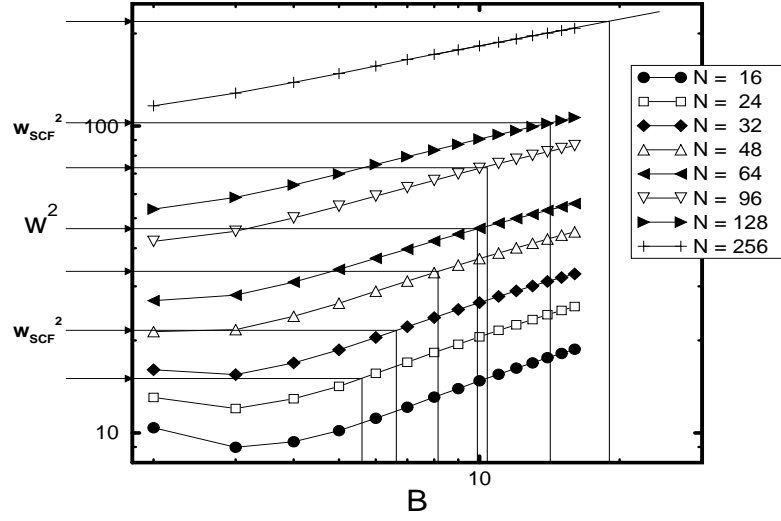
(b)
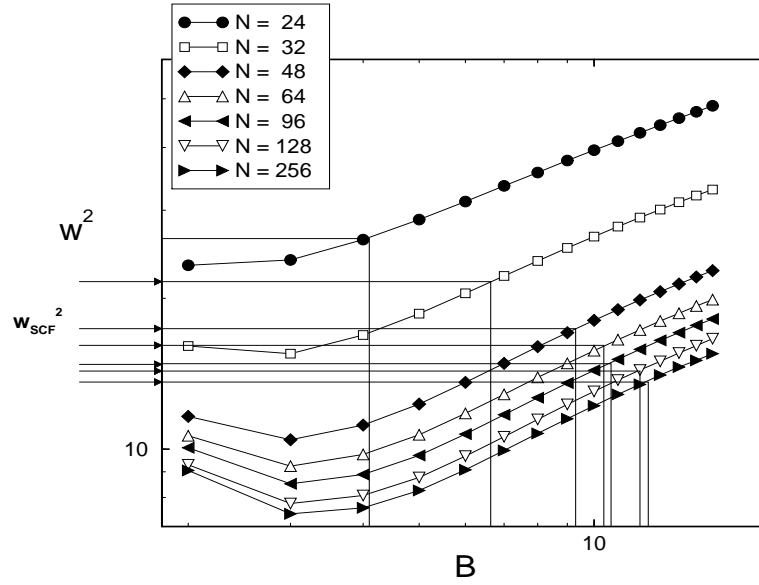
FIG. 10.

Squared apparent interfacial width w^2 as a function of block size B in absolute units (lattice constants) for different chain lengths and $\epsilon N = 0.96 = $ const. (a), $\epsilon = 0.03 = $ const. (b). Arrows indicate the self-consistent field predictions. They are used to read off the optimal block size B.

(a)
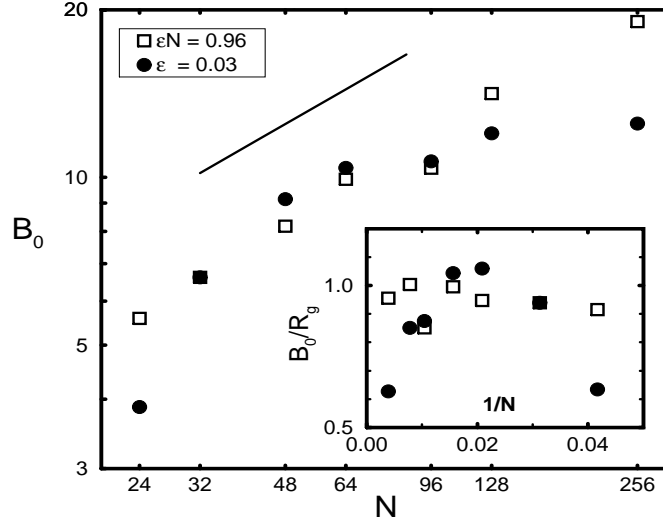
(b)
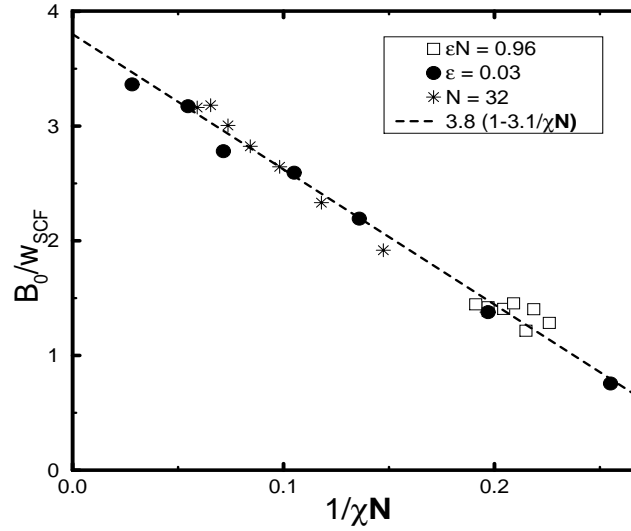
FIG. 11.

Optimal block size B_0 for different chain lengths N and ϵ for $\epsilon N = 0.96 = \mathrm{const.}$ (open squares), $\epsilon = 0.03 = \mathrm{const.}$ (filled circles), $N = 32 = \mathrm{const.}$ (stars), in absolute units as a function of chain length N (a), in units of R_g as a function of $1/N$ (inset in (a)), and in units of w_{SCF} as a function of $1/\chi N$ (b). Also shown in (a) is the slope $1/2$ ($\sqrt{N}$), and in (b) a fit of the data to $B = 3.8 w_{\mathrm{SCF}}(1 - 3.1/\chi N)$

19
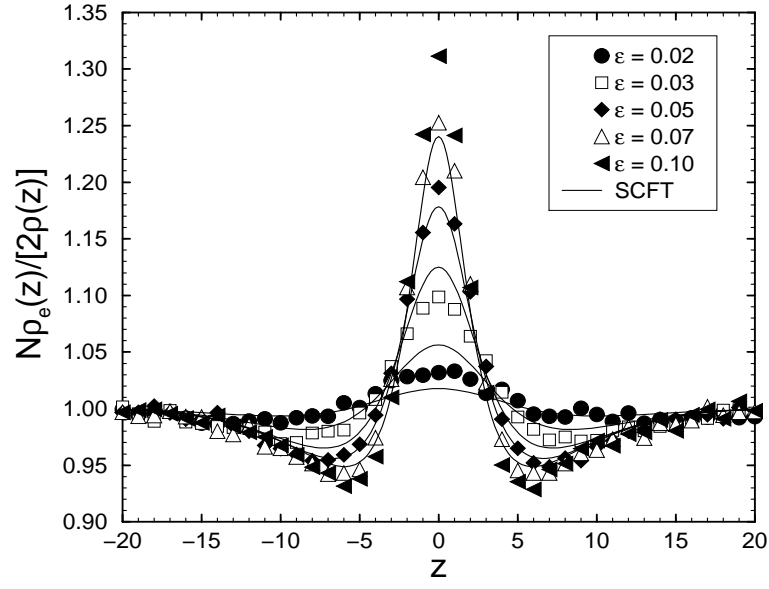
FIG. 12.
Normalized density of chain ends $\rho_e(z)$ vs. z in units of the lattice constant for chain length $N = 32$ and different ϵ. Profiles were taken at block size $B = 8$.
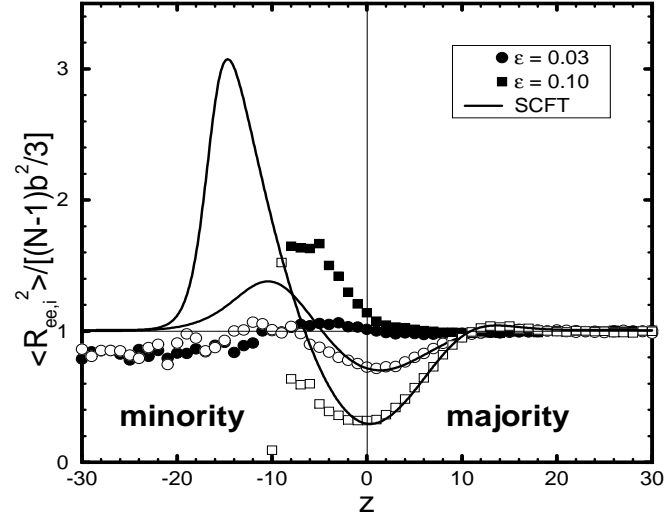
(a)
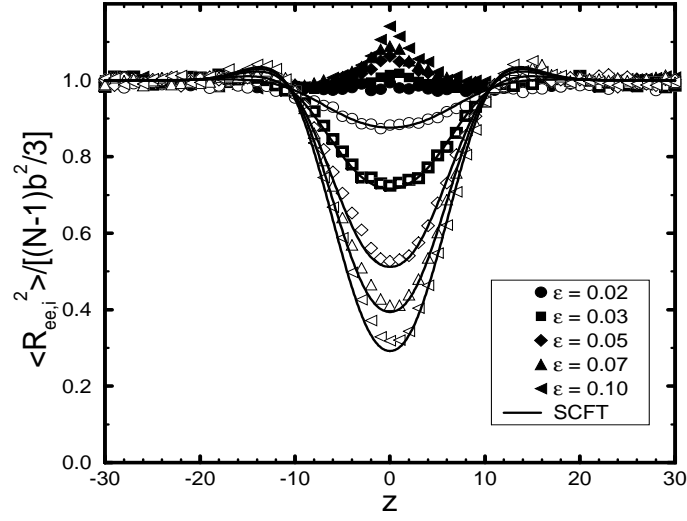
(b)

FIG. 13.

x/y components (filled symbols) and z components (open symbols) of the squared end-to-end vector $\langle R_{ee,i}{}^2 \rangle$ in units of the bulk value $b^2(N-1)/3$ as a function of the distance z of the midpoint from the center of the interface (in units of the lattice constant) for all chains, (a) and for A chains only (b). Parameters are $N = 32$, block size $B = 8$ and ϵ as indicated. Lines show the predictions of the self-consistent field theory.
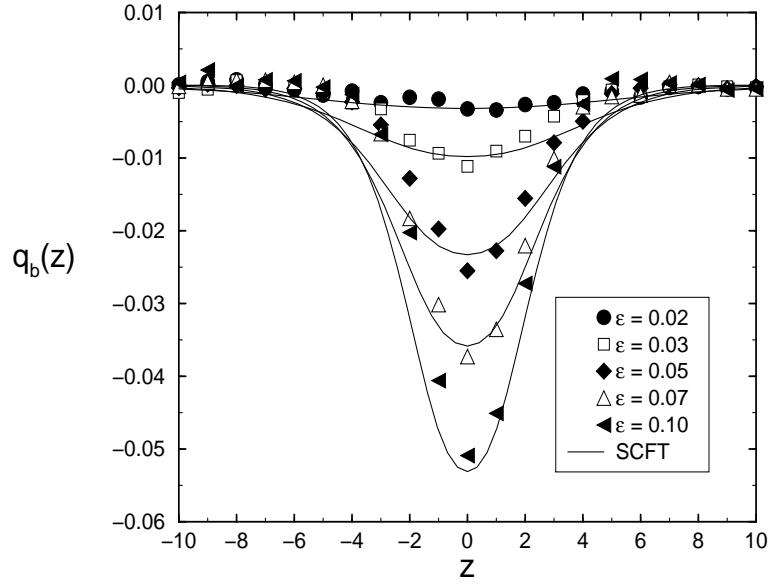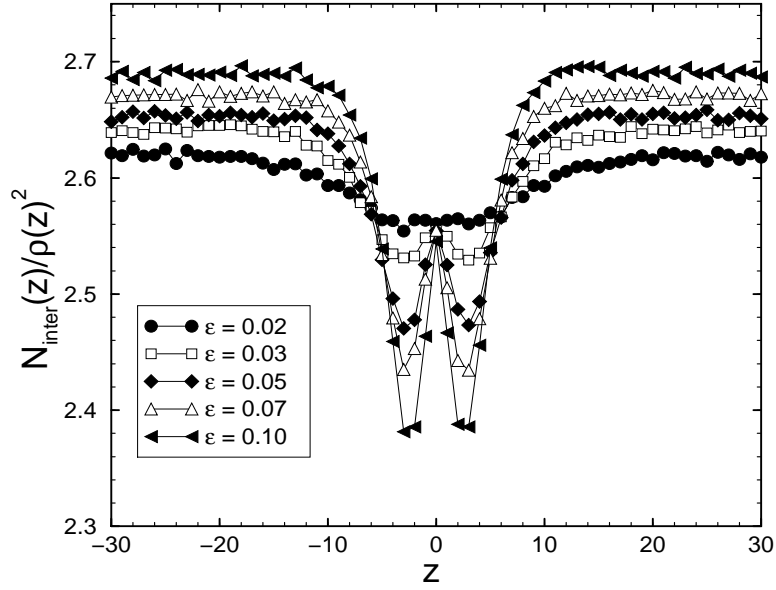
FIG. 14.

Bond orientational order parameter $q(z)$ vs. z in units of the lattice constant for chain length $N = 32$, block size $B = 8$, and ϵ as indicated. Lines show the predictions of the self-consistent field theory for a worm-like chain model with chain stiffness $\eta = 1.2$ (see text for explanation).
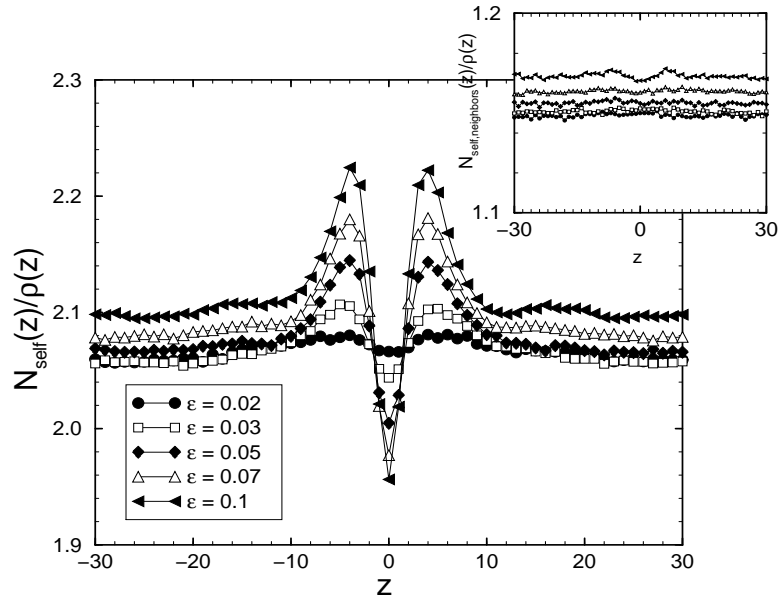
(a)

(b)

FIG. 15.

Profiles of (a) normalized number of interchain contacts $N_{inter}(z)/\rho(z)^2$ vs. z in units of the lattice constant and of (b) normalized number of self contacts $N_{self}(z)/\rho(z)$ vs. z . for different ϵ. Inset in (b) shows the number of contacts with direct neighbors along the chain. Parameters are $N = 32$ and $B = 8$.